Evolution of the structural and mean square displacement parameters in $(NH_4)_xK_{1-x}H_2PO_4$ solid solutions versus concentration and temperature

1998 J. Phys.: Condens. Matter 10 1621

(http://iopscience.iop.org/0953-8984/10/7/011)

J. Phys.: Condens. Matter **10** (1998) 1621–1641. Printed in the UK PII: S0953-8984(98)88044-2

Evolution of the structural and mean square displacement parameters in $(NH_4)_xK_{1-x}H_2PO_4$ solid solutions versus concentration and temperature

A Boukhris†§, M Souhassou†, C Lecomte†‖, B Wyncke† and A Thalal‡

† LCM^{3}B, URA CNRS 809, Université Henri Poincaré, Nancy 1, Faculté des Sciences, BP 239, 54506 Vandœuvre-lès-Nancy Cédex, France

‡ Département de Physique, Faculté des Sciences Semlalia, Marrakech, Morocco

Received 1 October 1997

Abstract. Accurate x-ray data sets were collected at different temperatures for mixed crystals of $(NH4)_xK_{1-x}H_2PO_4$ ($KADP_x$), where $x = 0.9$, 0.8, 0.5, 0.4 and 0.0. The phase transition temperatures of $KADP_{0.8}$ and $KADP_{0.9}$ were observed at $T_c = 109$ K and $T_c = 132$ K respectively. The vibration amplitudes are found to be larger for concentrations corresponding to the glassy phases. These large vibrations result from the static part of the mean square displacement which may be due to a static disorder due to a large difference between cell parameters of pure phases, or to fluctuations of the concentration throughout the crystal. In the range $0.23 < x < 0.75$, competition between the two H_2PO_4 configurations occurs (competition between the ferroelectric and antiferroelectric states): this leads to the observed static disorder of H_2PO_4 groups which prevents the phase transition from occurring.

1. Introduction

It is well known that potassium dihydrogen phosphate KH_2PO_4 (KDP) undergoes a para- to ferroelectric phase transition at 123 K [1–3], whereas ammonium dihydrogen phosphate $NH_4H_2PO_4$ (ADP) shows a para- to antiferroelectric phase transition at 148 K [4–7]. In the paraelectric phase, both compounds crystallize in the tetragonal system, space group $I\bar{4}2d$. After the transition, they become orthorhombic $Fdd2$ and $P2_12_12_1$ for KDP and ADP respectively. Mixed ferroelectric and antiferroelectric crystals show a glassy behaviour analogous to a spin-glass system in the intermediate concentrations; $RADP_x$ ($Rb_{1-x}(NH_4)_xH_2PO_4$) is the most intensively investigated [8] and $(NH_4)_xK_{1-x}H_2PO_4$ ($KADP_x$) has been established to be analogous to $RADP_x$, but less thoroughly studied. $KADP_x$ shows a ferroelectric phase transition for concentrations close to KDP ($x \leqslant 0.23$), and antiferroelectric for $x \geqslant 0.80$ (close to ADP). However, in contrast to $RADP_x$, the phase diagram is not known accurately [9, 10]. No phase transition was observed in the range $0.23 < x < 0.75$, and dielectric measurements on $KADP_{0.23}$ have shown the glassy low-frequency dispersion of dielectric constants [11]. Furthermore, structural studies have established that, for these intermediate concentrations, crystals remain in the paraelectric phase down to 20 K [9, 12] in agreement with infrared reflectivity studies [13]. However,

§ Permanent address: Département de Physique, Faculté des Sciences d'Agadir, Morocco.

‖ Author to whom correspondence should be addressed: lecomte@lcm3b.u-nancy.fr

0953-8984/98/071621+21$19.50

no x-ray or neutron structural analysis in the range $0.23 \leqslant x \leqslant 0.75$ has been carried out at any temperature for $KADP_x$.

The purpose of this paper is to describe single-crystal x-ray accurate structures of $KADP_x$ and to analyse the atomic mean square displacements versus temperature and concentration, with respect to KDP [15–17] and ADP [17, 18]. Therefore, we report in this paper the results of accurate x-ray diffraction, at three temperatures at least, on six single crystals of $(NH4)_xK_{1-x}H_2PO_4$, corresponding to $x = \{0.0, 0.4, 0.5, 0.8, 0.9$ [14], $1.0\}$. This study shows that thermal vibration of the phosphate group varies considerably with composition x, presenting a maximum at $x = 0.5$, which may be responsible for the glass phase behaviour, and therefore prevents the transition from occurring.

2. Experimental section

Crystals were grown from aqueous solution of ADP and KDP, at fixed temperature (295 K), by slow evaporation. The required ammonium concentration x was determined using the method of Ono *et al* [9]. Because of the non-linear variation of the concentration in aqueous solutions versus solid solutions [9], crystals used for x-ray diffraction were selected at the very beginning of the crystallization process to avoid any fluctuation in the concentration through the crystal. Only crystals that presented an appropriate size, habit and fine diffraction spots on a Weissenberg camera were selected. As expected, the cell parameter c varied with the concentration, which permitted us to check the concentration x for the crystallized materials as shown in figure 1: from this graph, we found that our samples had x very close to the required concentration $x = \{0.0, 0.4, 0.5, 0.8, 0.9, 1.0\}$; all solid solutions present approximately the same habits as ADP and KDP, with {100}, {010}, {101} and {011} crystal forms. For $x = 0.6$ and $x = 0.7$, no good-quality crystals suitable for accurate x-ray data were obtained, and therefore they were not used in this study.

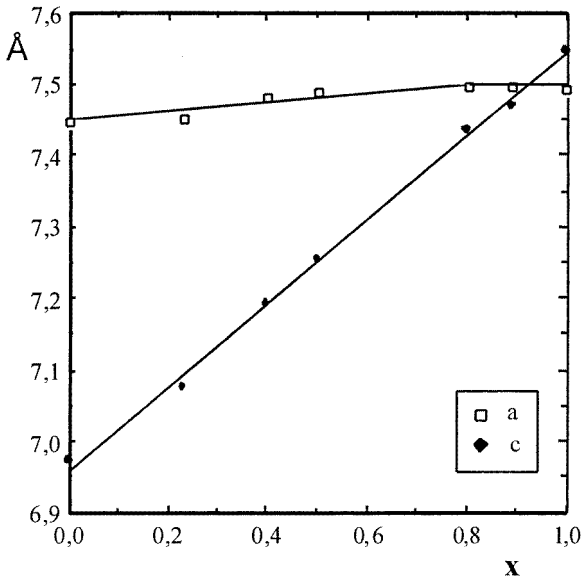

Figure 1. Variation of cell parameters with ammonium concentration x.

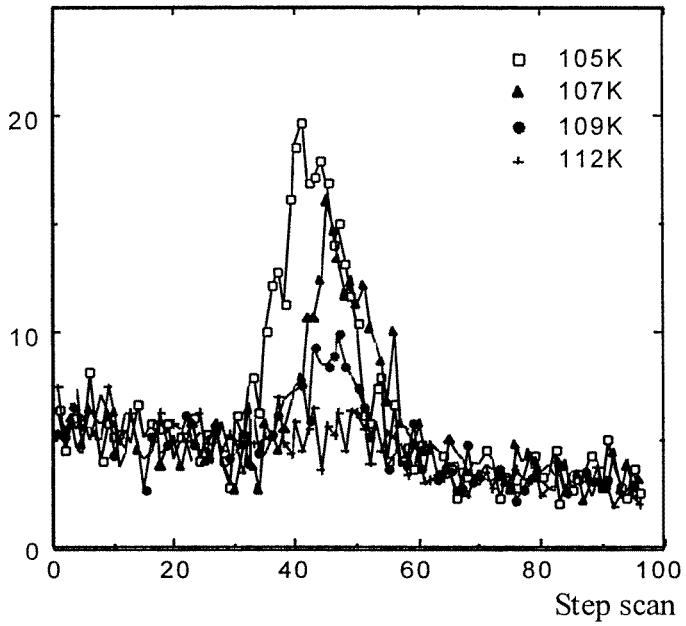

(a)

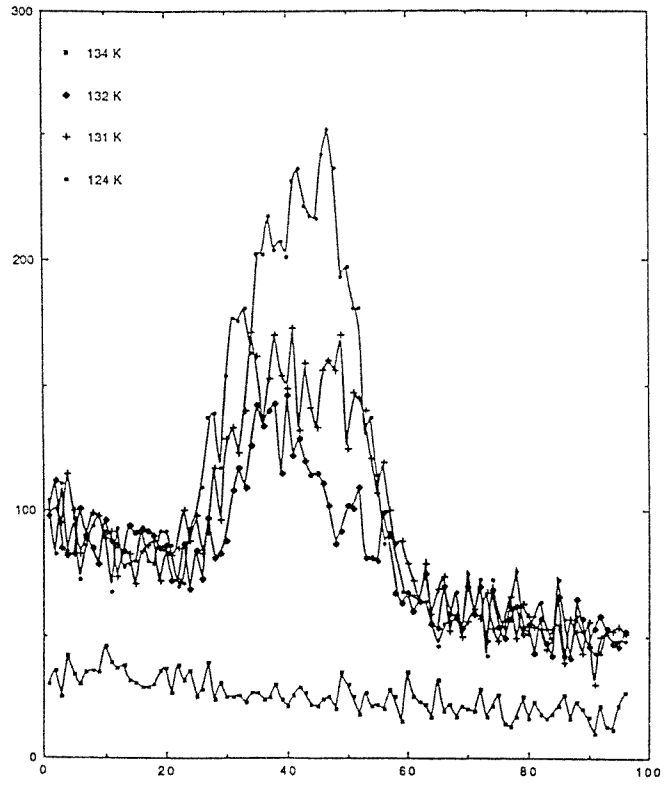

(b)

Figure 2. Profiles of the (012) reflection against temperature (K): (a) $KADP_{0.8}$; (b) $KADP_{0.9}$.

Table 1. Details of data collection.

Formula	$K_{1-x}(NH_4)_xH_2PO_4$						
Space group	$I\bar{4}2d$						
Diffractometer	CAD4F Enraf Nonius						
Radiation	Mo(Kα) (0.7107 Å)						
Scan	ω–2θ						
Z	4						
Concentration	$x = 0.4$			$x = 0.5$			
Molecular weight (g)	127.66			125.66			
Crystal volume (mm^3)	10.6×10^{-3}			13.2×10^{-3}			
$\Delta\omega$	$1.15 + 0.35\tan\theta$			$1.2 + 0.35\tan\theta$			
μ (mm^{-1})	1.16			1.06			
	105 K	158 K	295 K	105 K	158 K	295 K	
a (Å)	7.451(1)	7.458(1)	7.482(1)	7.456(1)	7.463(1)	7.489(1)	
c (Å)	7.145(2)	7.162(2)	7.192(1)	7.214(2)	7.226(2)	7.255(2)	
V ($Å^3$)	396.7(1)	398.3(1)	402.6(1)	401.0(1)	402.5(1)	406.8(1)	
$(\sin\theta/\lambda)_{max}$ ($Å^{-1}$)	1.27	1.27	1.27	1.27	1.27	1.32	
Measured reflections	2002	1999	1977	2038	2429	2274	
Unique reflections ($I \geqslant 3\sigma(I)$)	685	632	485	699	645	531	
Scan speed (° mm^{-1})	$1.18 < v < 2.75$			$1.37 < v < 2.75$			
hkl limit	$0 \leqslant h \leqslant 18, 0 \leqslant k \leqslant 18, 0 \leqslant l \leqslant 17$			$0 \leqslant h \leqslant 18, 0 \leqslant k \leqslant 18, 0 \leqslant l \leqslant 19$			
Control reflections	(0 8 0), (8 0 4), (0 8 4), (8 0 0)			(0 8 2), (8 0 4), (0 8 4), (8 0 0)			
Concentration	$x = 0.8$			$x = 0.9$			
Molecular weight (g)	117.63			117.13			
Crystal volume (mm^3)	8.7×10^{-3}			8.8×10^{-3}			
$\Delta\omega$	$1.0 + 0.35\tan\theta$			$1.0 + 0.35\tan\theta$			
μ (mm^{-1})	0.73			0.62			
	125 K	158 K	295 K	154 K	164 K	192 K	295 K
a (Å)	7.462(1)	7.470(1)	7.499(1)	7.469(1)	7.471(1)	7.473(2)	7.497(1)
c (Å)	7.409(1)	7.417(1)	7.436(1)	7.456(3)	7.457(3)	7.462(3)	7.471(3)
V ($Å^3$)	412.5(1)	413.9(1)	418.1(1)	415.9(1)	416.2(1)	416.7(1)	419.9(1)
$(\sin\theta/\lambda)_{max}$ ($Å^{-1}$)	1.27	1.27	1.27	1.15	1.22	1.22	1.29
Measured reflections	3209	2065	2196	1552	1828	1875	2290
Unique reflections ($I \geqslant 3\sigma(I)$)	638	730	553	575	629	586	492
Scan speed (° mm^{-1})	$0.86 < v < 2.75$			$1.10 < v < 2.75$			
hkl limit	$0 \leqslant h \leqslant 19, 0 \leqslant k \leqslant 19, 0 \leqslant l \leqslant 18$			$0 \leqslant h \leqslant 19, 0 \leqslant k \leqslant 19, 0 \leqslant l \leqslant 19$			
Control reflections	(8 0 0), ($\bar{1}$ 0 0), (0 8 0), (0 $\bar{8}$ 0)			(4 0 0), (0 4 0), (4 0 6), (5 $\bar{1}$ 6)			

Two of these mixed crystals $x = 0.9$ [14] and 0.8 undergo an antiferroelectric phase transition at 132 and 109 K respectively, as shown by the presence and the growth of the (012) forbidden reflection with temperature (figure 2). The small shift in the scan position is due to the change in cell parameters. The profiles of the forbidden reflections for both concentrations present the same feature: a sudden appearance of the reflection as a function of temperature which is a characteristic of a first-order transition. The transition is reversible as long as the crystal is small enough to avoid existence of domains which lead to destruction of the crystal after the transition. Determination of the high-resolution structure of the antiferroelectric phases is in progress and will be published later.

Table 2. Internal agreement factors between symmetry equivalent reflections (I, calculated without absorption corrections; II, calculated with absorption correction):

$$R = \left(\sum_i |I_i - \langle I\rangle|\right)\left(\sum_i I_i\right)^{-1}$$

$$R_w = \left(\sum_i w_i (I_i - \langle I\rangle)^2\right)\left(\sum_i w_i I_i\right)^{-1}$$

$$w_i = \frac{1}{\sigma(I_i)^2} \qquad R_2 = R_w \text{ with } w = 1$$

N_{Term} is the total number of measured reflections, N_{Uniq} is the number of unique reflections, A_{min} and A_{max} are the minimum and the maximum absorption.

x	T (K)		R_1 (%)	R_2 (%)	R_w (%)	N_{Term}	N_{Uniq}	N_{Uniq} $I > 3\sigma(I)$	$A_{min} - A_{max}$
0.4	105	I	2.19	2.63	3.17	1894	939	685	0.756–0.790
		II	2.11	2.53	3.07				
	158	I	2.33	2.79	3.03	1888	993	632	
		II	2.30	2.69	2.93				
	295	I	2.44	2.57	3.05	1870	1002	485	
		II	2.33	2.34	2.97				
0.5	105	I	4.23	5.39	4.46	1924	1004	700	0.749–0.814
		II	2.30	2.87	3.62				
	158	I	3.65	4.99	3.59	2352	974	645	
		II	2.41	3.64	2.97				
	295	I	3.63	4.94	3.51	2100	1116	531	
		II	1.59	2.17	2.03				
0.8	125	I	2.21	1.93	2.37	3079	1002	638	0.850–0.869
		II	2.16	1.84	2.35				
	158	I	0.96	0.86	1.87	1945	980	730	
		II	0.89	0.66	1.83				
	295	I	1.06	1.13	1.76	2079	991	553	
		II	0.88	0.76	1.68				
0.9	154	I	1.66	1.84	3.09	1552	756	594	0.847–0.901
		II	1.25	1.20	2.70				
	164	I	1.67	1.81	3.09	1828	886	650	
		II	1.32	1.20	2.71				
	192	I	2.00	2.23	2.82	1875	887	605	
		II	1.36	1.00	2.47				
	295	I	2.37	2.37	2.79	2290	1130	506	
		II	1.33	0.89	2.22				

For each of these concentrations, we measured x-ray diffraction data in the paraelectric phase at three different temperatures at least, using a CAD4F Enraf Nonius [19] diffractometer equipped with a liquid nitrogen vapour stream apparatus installed in a dry box to prevent ice formation. The gas stream temperature was maintained constant within 1 K as monitored by a copper–constantan thermocouple positioned 5 mm upstream from the crystal. The temperature was calibrated using the transition temperature of ADP (148 K) and KDP (123 K). All the data were measured using graphite monochromated Mo(Kα) radiation with an $\omega/2\theta$ scan; the width scanned is defined as $\Delta\omega = a + 0.35\tan(\theta)$, where a is a variable depending mainly on the crystal mosaicity and on the divergence of the beam. The values of the a parameter which therefore depends on the crystal quality was found to be sensitive to the x concentration, larger in glassy phases ($a = 1.15^\circ$, 1.20° for $x = 0.4$, 0.5 respectively) compared to $a = 1^\circ$ for the other concentrations studied. This

latter value is equal to that used for the pure ADP phase [18]. Details of the data collection are summarized in table 1.

3. Data reduction

Data reduction and error analysis were performed using Blessing's programs DREAR [20], and Gaussian quadrature absorption correction was applied with program Absorb [21]. Data were measured, at least, at a resolution of 1.15 Å^{-1} ($\sin\theta/\lambda$), and half the Ewald sphere was measured in each case. As shown in table 2, the absorption correction improved well the statistical agreements between equivalent reflections. This correction goes from 1% to 6% and the internal agreement factors are given in table 2. The intensity variances were calculated according to McCandlish *et al* [22]; $\sigma^2(|F|^2) = \sigma_c^2(|F|^2) + p(|F|^2)$ where $\sigma_c^2(|F|^2)$ accounts for Poisson statistics and p is an instrumental factor ($0.00 < p < 0.023$).

For $x = 0.8$, the internal agreement increases from $R_1 = 0.89\%$ ($T = 158$ K) to 2.16% at $T = 125$ K. This is probably due to the fact that we are approaching the transition temperature ($T_c = 109$ K) ; therefore, the crystal starts to present domains that have already transited (domains which should be very small compared to the rest of the crystal). These domains could be microdomains in which the x concentration is slightly higher than 0.8 (non-homogeneity of the crystals).

4. Crystal structure refinements

The structures of $(NH_4)_xK_{(1-x)}H_2PO_4$ ($x = 0.4$, 0.5, 0.8, 0.9, 1), were determined and refined with SHELX [23] and NRCVAX [24] programs; hydrogen atoms were found by Fourier difference maps. Position and displacement parameters of non-hydrogen atoms were refined at high order ($\sin\theta/\lambda \geqslant 0.8$ Å^{-1}). Hydrogen atoms were refined using low-order data. We found a high correlation between the U^{ij} of the potassium and the ammonium nitrogen atoms, because they occupy the same site $(0, 0, 1/2)$; so, different strategies were adopted in order to determine their thermal parameters and the concentration x: the concentration was determined from the variation of the $\boldsymbol{c}$ parameter (figure 1) and was fixed at the first stage of the refinements; U^{ij} of K and N atoms were refined independently at high angles. After convergence, the N and K occupancies were refined. Another strategy was the use of a mixed form factor, which consists of a weighted sum of the form factors of N and K atoms. This led to U^{ij} values of the average atom statistically equal to the weighted average of those found for N and K separately.

Then, in order to better deconvolute anisotropic mean square displacement parameters from the aspherical atomic electron density, a multipolar analysis of the density was performed, using separate N and K atoms. The multipole refinement consists in expanding the electron density around each centre, according to the Hansen–Coppens model [25]:

$$\rho(\boldsymbol{r}) = \rho_c(r) + P_v\kappa^3\rho_v(\kappa r) + \sum_{lm} P_{lm}\kappa'^3 R_{nl}(\kappa' r)\, y_{lm}(\theta, \phi) \tag{1}$$

where $R_{nl}(r) = N r^{nl}\, \mathrm{e}^{-\kappa'\alpha r}$ is a Slater type radial function which has an extension big enough to take into account the bonding electron density, and $y_{lm}(\theta, \phi)$ are real spherical harmonics; $\rho_c(r)$ and $\rho_v(r)$ are spherical core and valence electron distributions, obtained using Clementi [26] wavefunctions for isolated atoms, P_v is the number of valence electrons. The κ and κ' are radial expansion/contraction coefficients of the spherical and aspherical valence deformation densities respectively. By developing the density in this way, we can

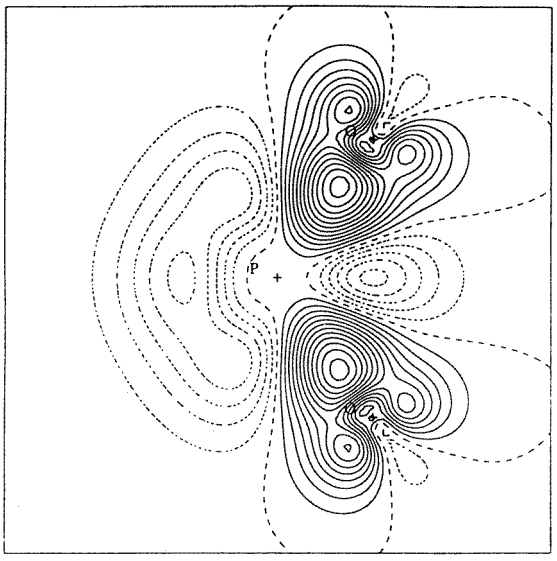

(a)

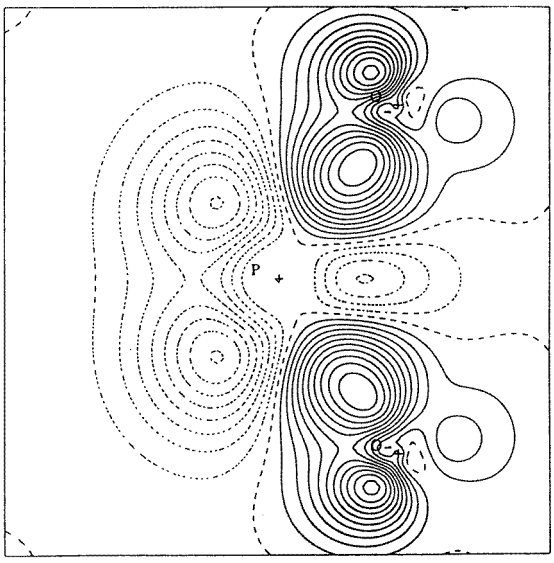

(b)

Figure 3. Static deformation electron density maps calculated at 158 K: (a) $KADP_{0.8}$ and (b) ADP. Contour level is 0.05 e^- $Å^{-3}$.

take into account the fact that electron density around each atom is not spherical because of interatomic interactions.

As we had a very good data set for $x = 0.8$ (see table 2), we have performed a multipolar refinement against these very accurate data at ($T = 125$, 158 and 295 K). The resulting static model deformation density maps calculated as

$$\Delta\rho(\boldsymbol{r}) = P_v\kappa^3\rho_v(\kappa r) - N_v\rho_v(r) + \sum_{lm}\kappa'^3 R_{nl}(\kappa' r)P_{lm}y_{lm}(\theta,\phi) \qquad (2)$$

Table 3. Fractional coordinates and thermal parameters of the atoms for the $KADP_{0.8}$ compound: (a) independent atom model refinements, (b) refinements using multipolar density P_{lm} parameters of $KADP_{0.8}$ at 158 K. Statistics of the refinements: $R(F) = \Sigma\Delta/\Sigma k^{-1}|F_0|$, $R_w(F) = (\chi^2/\Sigma w F_0^2)^{1/2}$ and $S = (\chi^2/(N - N_{par}))^{1/2}$, where $\chi^2 = \Sigma w \Delta^2$, $\Delta = |k^{-1}|F_0| - |F_0||$, $w = 1/\sigma^2(F_0)$ and N_0 and N_{par} are respectively the number of data and the number of refined parameters. x is the site occupancy and k is the scale factor.

		$T = 125$ K		$T = 158$ K	$T = 295$ K	
Atom	Parameter	(a)	(b)	(b)	(a)	(b)
N	U^{11}	0.016 02(21)	0.015 96(13)	0.018 01(13)	0.030 77(22)	0.030 21(13)
	U^{33}	0.012 97(49)	0.014 01(34)	0.015 86(31)	0.023 43(51)	0.025 45(30)
K	U^{11}	0.014 33(10)	0.014 42(11)	0.016 81(9)	0.029 52(10)	0.029 85(12)
	U^{33}	0.012 20(26)	0.012 02(28)	0.015 17(20)	0.025 16(23)	0.024 21(30)
P	U^{11}	0.006 12(4)	0.006 20(4)	0.007 84(3)	0.014 04(4)	0.014 06(3)
	U^{33}	0.019 74(11)	0.019 77(10)	0.020 72(7)	0.028 60(8)	0.028 70(7)
O	x	0.147 96(6)	0.147 97(4)	0.147 80(4)	0.146 73(6)	0.146 59(3)
	y	0.084 31(7)	0.084 37(4)	0.084 47(4)	0.084 50(6)	0.084 58(3)
	z	0.117 34(10)	0.117 39(5)	0.117 32(6)	0.117 31(9)	0.117 14(4)
	U^{11}	0.009 95(12)	0.010 00(9)	0.012 02(8)	0.021 25(14)	0.021 30(9)
	U^{22}	0.009 11(12)	0.008 92(9)	0.010 91(8)	0.019 41(14)	0.019 22(9)
	U^{33}	0.022 22(19)	0.022 44(14)	0.024 33(12)	0.037 18(21)	0.036 79(11)
	U^{12}	0.000 68(5)	0.000 63(4)	0.000 80(3)	0.001 63(6)	0.001 65(4)
	U^{13}	−0.002 18(9)	−0.002 15(6)	−0.002 67(5)	−0.004 90(10)	−0.004 67(5)
	U^{23}	−0.001 44(8)	−0.001 37(6)	−0.001 65(5)	−0.003 22(9)	−0.003 06(5)
H(O)	x	0.150(2)	0.139(2)	0.133(2)	0.141(1)	0.133(1)
	y	0.214(2)	0.225(3)	0.224(2)	0.213(1)	0.224(2)
	z	0.116(4)	0.096(5)	0.100(4)	0.111(2)	0.119(2)
	U	0.023(5)	0.023(5)	0.031(4)	0.028(3)	0.035(3)
H(N)	x	0.014(2)	−0.001(3)	0.001(2)	0.016(1)	0.007(2)
	y	0.085(2)	0.102(2)	0.105(2)	0.088(1)	0.099(1)
	z	0.433(1)	0.411(1)	0.414(1)	0.441(1)	0.418(1)
	U	0.034(5)	0.038(4)	0.043(3)	0.056(2)	0.058(3)
	k	0.8379(5)	0.8414(8)	1.7157(7)	1.7181(6)	1.7211(13)
	$R(F)$ (%)	1.68	1.76	1.32	1.23	1.34
	$R_w(F)$ (%)	1.38	1.48	1.10	0.82	0.97
	G.O.F.	0.78	0.84	1.06	0.96	1.14
	x	0.805(2)	0.808(2)	0.807(1)	0.806(2)	0.808(2)

with N_v = number of valence electrons of the free neutral atom compared to those calculated for ADP [18, 27] did not show any significant differences: the $KADP_{0.8}$, static deformation map calculated from 158 K data (figure 3) reveals bonding P–O and lone pair density equal to those obtained from the ADP data within standard deviations ($\sigma(\Delta\rho) \approx 0.05$ e$^-$ Å^{-3}). Therefore we transferred the multipolar density P_{lm} parameters of $KADP_{0.8}$ at 158 K to all other structures ($x = 0.4$, 0.5 and 0.9) at different temperatures. This transfer consists in assigning an aspherical electron density to P, O, N and H atoms, and by Fourier transformation of (1) we obtain the form factors as follows (Lecomte [25]):

$$f(\boldsymbol{H}) = f_{IAM}(H) + \delta f(\boldsymbol{H})$$
$$\delta f(\boldsymbol{H}) = P_v f_v\left(\frac{H}{\kappa}\right) + \sum_{lm} P_{lm}\Phi_{nl}\left(\frac{H}{\kappa'}\right) Y_{lm\pm}\left(\frac{\boldsymbol{H}}{H}\right) \qquad (3)$$

Table 4. Fractional coordinates and thermal parameters of the atoms for $KADP_x$ compounds ($x = 0.4$, 0.5, 0.9) from refinements using multipolar density P_{lm} parameters of $KADP_{0.8}$ at 158 K.

		$KADP_{0.4}$			$KADP_{0.5}$			$KADP_{0.9}$			
Atom	Parameter	105 K	158 K	295 K	105 K	158 K	295 K	154 K	164 K	192 K	295 K
N	U^{11}	0.0118(3)	0.0155(4)	0.0279(7)	0.0114(2)	0.0153(2)	0.0266(6)	0.016 65(13)	0.017 51(13)	0.019 58(14)	0.028 62(21)
	U^{33}	0.0154(7)	0.0191(9)	0.0355(18)	0.0144(4)	0.0198(6)	0.0312(15)	0.013 15(34)	0.013 17(34)	0.016 27(37)	0.023 05(53)
K	U^{11}	0.010 61(5)	0.014 31(6)	0.025 51(10)	0.011 37(4)	0.015 02(5)	0.026 18(12)	0.016 48(27)	0.017 04(29)	0.019 87(30)	0.028 47(50)
	U^{33}	0.013 96(10)	0.017 20(12)	0.024 52(20)	0.014 56(10)	0.016 22(13)	0.025 47(30)	0.014 54(72)	0.014 85(77)	0.018 22(84)	0.024 00(143)
P	U^{11}	0.005 61(4)	0.007 65(4)	0.013 23(6)	0.005 68(4)	0.007 46(4)	0.013 00(10)	0.007 63(5)	0.008 02(5)	0.009 35(5)	0.013 64(7)
	U^{33}	0.027 09(14)	0.028 45(15)	0.032 78(19)	0.028 65(13)	0.030 40(13)	0.037 07(24)	0.018 44(11)	0.018 87(12)	0.020 60(11)	0.026 14(14)
O	x	0.148 51(4)	0.148 21(4)	0.147 34(6)	0.148 42(4)	0.148 07(4)	0.147 14(7)	0.147 82(5)	0.147 76(5)	0.147 54(4)	0.146 76(6)
	y	0.083 71(4)	0.083 80(4)	0.083 77(6)	0.083 92(4)	0.083 99(4)	0.084 20(8)	0.084 55(5)	0.084 51(5)	0.084 61(5)	0.084 70(7)
	z	0.122 39(8)	0.122 24(9)	0.121 69(10)	0.121 10(7)	0.120 88(7)	0.120 06(12)	0.116 25(6)	0.116 28(7)	0.116 28(6)	0.116 15(8)
	U^{11}	0.008 15(7)	0.010 72(8)	0.018 99(14)	0.008 40(7)	0.010 88(9)	0.018 34(22)	0.011 62(12)	0.012 29(11)	0.013 84(11)	0.020 56(18)
	U^{22}	0.007 84(7)	0.010 42(8)	0.017 81(13)	0.008 11(7)	0.010 37(9)	0.017 08(21)	0.010 58(12)	0.011 05(11)	0.012 69(12)	0.018 87(18)
	U^{33}	0.027 10(15)	0.030 39(18)	0.039 40(25)	0.028 83(14)	0.032 16(16)	0.043 95(34)	0.022 04(17)	0.022 87(18)	0.025 69(17)	0.035 76(28)
	U^{12}	0.000 37(3)	0.000 62(4)	0.001 27(6)	0.000 39(3)	0.000 67(4)	0.001 27(9)	0.000 75(5)	0.000 83(5)	0.000 87(5)	0.001 58(8)
	U^{13}	−0.001 57(6)	−0.002 07(7)	−0.003 72(10)	−0.001 63(6)	−0.002 18(6)	−0.003 76(15)	−0.002 59(7)	−0.002 84(7)	−0.003 18(7)	−0.004 89(11)
	U^{23}	−0.001 15(5)	−0.001 59(6)	−0.002 64(10)	−0.001 13(5)	−0.001 48(6)	−0.002 60(14)	−0.001 56(7)	−0.001 65(7)	−0.001 98(7)	−0.003 03(11)
H(O)	x	0.161(5)	0.161(5)	0.156(4)	[a]	0.146(3)	[a]	0.126(4)	0.129(4)	0.124(3)	0.125(4)
	y	0.218(5)	0.218(5)	0.223(4)	[a]	0.226(3)	[a]	0.228(3)	0.228(4)	0.226(3)	0.225(4)
	z	0.085(5)	0.089(7)	0.102(8)	[a]	0.114(5)	[a]	0.134(4)	0.143(3)	0.139(3)	0.137(4)
	U	0.034(7)	0.038(9)	0.052(8)	0.020(6)	0.034(5)	0.044(5)	0.026(6)	0.029(7)	0.028(6)	0.043(8)
H(N)	x	−0.009(5)	−0.009(8)	−0.005(7)	[a]	−0.010(6)	[a]	0.011(3)	−0.011(3)	−0.008(2)	−0.002(4)
	y	0.107(6)	0.094(8)	0.121(8)	[a]	0.105(6)	[a]	0.111(3)	0.104(3)	0.106(2)	0.106(3)
	z	0.422(4)	0.418(5)	0.431(8)	[a]	0.417(2)	[a]	0.415(1)	0.414(1)	0.414(1)	0.412(2)
	U	0.044(7)	0.049(10)	0.057(9)	0.057(9)	0.069(7)	0.071(7)	0.049(4)	0.055(5)	0.048(3)	0.054(6)
	k	1.896(1)	1.665(1)	1.896(2)	1.893(2)	2.129(2)	2.161(3)	1.2845(9)	1.2875(9)	1.2946(8)	1.2586(9)
	$R(F)$	1.82	1.79	1.83	2.17	1.84	2.82	1.81	2.06	2.08	2.29
	$R_w(F)$	1.88	1.92	1.95	2.56	2.07	2.78	1.73	1.83	1.47	1.62
	G.O.F.	1.04	0.94	1.02	0.94	1.06	2.16	1.38	1.33	1.36	1.44
	N_{obs}	685	632	485	699	645	531	575	629	586	492
Conc.	(x)	0.4	0.4	0.4	0.5	0.5	0.5	0.897(2)	0.899(2)	0.899(2)	0.907(3)

[a] Same fractional coordinates as $KADP_{0.5}$ at 158 K.

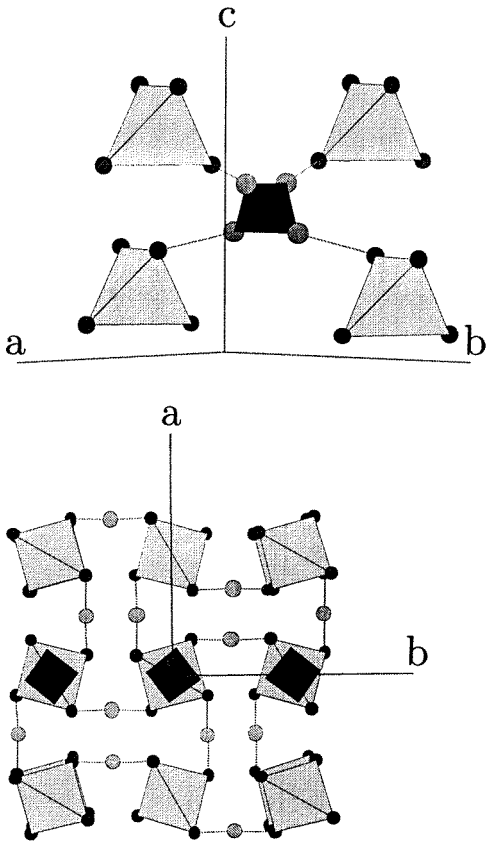

Figure 4. Crystal structure of ADP projected on the $\boldsymbol{a}$, $\boldsymbol{b}$ plane (paraelectric phase). Black and grey tetrahedra are NH_4 and PO_4 entities respectively.

where

$$\Phi_{nl}(H) = 4\pi \mathrm{i}^l \int_0^\infty R_{nl}(r) J_l(2\pi H r) r^2 \, \mathrm{d}r.$$

f_{IAM} is the usual independent atom model form factor. The P_v, κ, κ' and P_{lm} parameters were fixed at the 158 K $KADP_{0.8}$ values and never refined. This strategy led to very precise thermal parameters of the PO_4 group. Tables 3 and 4 give the summary of the refinements for $KADP_x$ ($x = 0.8$ and $x = 0.4$, 0.5 and 0.9) respectively. Multipole parameters are available on request to the authors (lecomte@lcm3b.u-nancy.fr).

5. Structural results

In this section, we will discuss our structural results compared to those concerning KDP [17] and ADP [18].

In the paraelectric phase, the KDP structure consists of a network of PO_4 tetrahedra that are linked by very short hydrogen bonds. These hydrogen bonds are almost parallel to the $\boldsymbol{a}$ and $\boldsymbol{b}$ axes. The potassium is surrounded by six phosphate tetrahedra in a distorded octahedron fashion, two being above and below along the $\boldsymbol{c}$ axis. ADP has the same structure

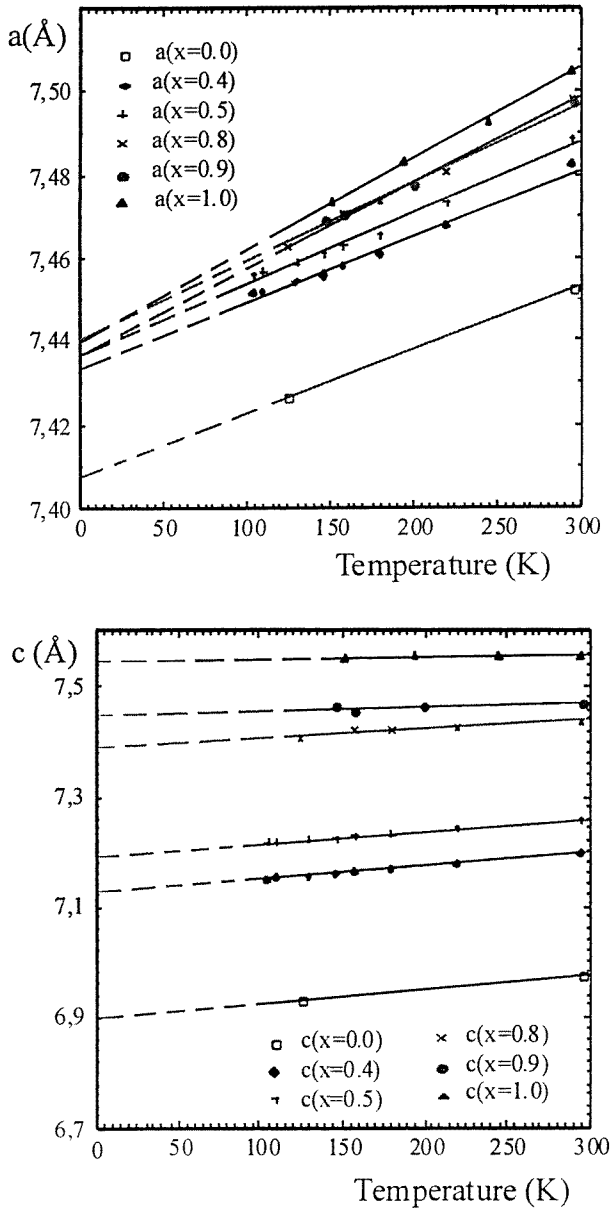

Figure 5. Variation of cell parameters with temperature.

(figure 4) except that the potassium cation is replaced by the ammonium tetrahedron which is therefore linked to phosphate tetrahedra via hydrogen bonds [28]. There is a very small difference between the cell parameters $\boldsymbol{a}$ of ADP and KDP, in contrast to $\boldsymbol{c}$ which varies by about 0.5 Å, because of the large difference between the ionic radius of K^+ and NH_4^+ (1.33 and 1.42 Å respectively). So, the $\boldsymbol{a}$ parameter is almost independent of the x concentration, while $\boldsymbol{c}$ varies linearly with concentration x, in agreement with Ono *et al* [9, 11].

5.1. Cell parameters versus temperature

Table 5 gives the variation of the cell parameters with temperature and concentration x. As shown in figure 5 cell parameters decrease linearly with decreasing temperature. This contraction is also dependent on the concentration. The linear thermal expansion, along the $\boldsymbol{a}$ axis defined as

$$\alpha_a = \frac{\mu_a}{a} \text{ with } \mu_a = \frac{\partial a}{\partial T}$$

increases very little with the concentration (from 20×10^{-6} to 29×10^{-6} K^{-1}) (table 6); then the rate of change is hardly dependent on the concentration as expected.

Table 5. Cell parameters against concentration and temperature.

Temperature	$x = 0.4$		$x = 0.5$		$x = 0.8$		$x = 0.9$	
(K)	a (Å)	c (Å)	a (Å)	c (Å)	a (Å)	c (Å)	a (Å)	c (Å)
105	7.451(1)	7.145(2)	7.456(1)	7.214(2)				
110	7.452(1)	7.151(2)	7.457(1)	7.215(2)				
125					7.462(1)	7.409(1)		
130	7.454(1)	7.155(2)	7.459(1)	7.219(2)				
147	7.456(1)	7.159(2)	7.460(1)	7.223(2)				
154							7.469(1)	7.456(3)
158	7.458(1)	7.162(2)	7.463(1)	7.226(2)	7.470(1)	7.417(1)		
164							7.471(1)	7.457(3)
170			7.465(1)	7.228(2)				
180	7.460(1)	7.166(2)	7.466(1)	7.230(2)	7.474(1)	7.421(1)		
192							7.473(2)	7.462(3)
200			7.470(1)	7.236(1)				
220	7.467(1)	7.176(1)	7.473(1)	7.241(1)	7.481(1)	7.427(1)		
234					7.484(1)	7.430(1)		
295	7.482(1)	7.192(1)	7.489(1)	7.255(1)	7.499(1)	7.436(1)	7.497(1)	7.471(3)

Table 6. Thermal expansion/contraction against ammonium concentration x.

Parameter	Coefficient	$x = 0$	$x = 0.4$	$x = 0.5$	$x = 0.8$	$x = 0.9$	$x = 1.0$
a	μ_a (10^{-4}) Å K^{-1}	1.51	1.60	1.73	2.06	1.90	2.21
	α_a (10^{-6}) K^{-1}	20	21	23	26	25	29
c	μ_c (10^{-4}) Å K^{-1}	2.53	2.36	2.19	1.57	0.80	0.52
	α_c (10^{-6}) K^{-1}	36	33	30	21	11	6.6

Along the $\boldsymbol{c}$ axis, as a function of x, α_c decreases non-linearly by a large amount from 36×10^{-6} K^{-1} to 7×10^{-6} K^{-1}, i.e. 500% (table 6). For a high ammonium concentration, the change in $\boldsymbol{c}$ with temperature is small, and for low concentration the change is larger. This is due to the type of interaction between ammonium or potassium cations with the PO_4 anions. For KDP, the interaction is ionic, and therefore the $K \ldots PO_4$ distance is more temperature dependant than the $NH_4 \ldots PO_4$ distance in ADP where the interaction is a combination of ionic and hydrogen bond interactions: because of the hydrogen bonds, the rate of change is small; in addition, the ammonium group has a larger ionic radius than that of the potassium cation.

5.2. Variation of the stereochemical parameters with temperature

Table 7 shows the evolution of the main distances and angles as a function of temperature and concentration. For the sake of comparison, table 8 shows the values of these distances and angles calculated for ADP and KDP. At first, we see that the bond distances and angles show similar behaviour as a function of T whatever the concentration: the distance P–O does not change within standard deviations as already stated by Nelmes *et al* [15, 16] for KDP in a temperature and pressure dependent study. The $O^a \ldots O^i$ distance (short hydrogen bond) (see tables 7 and 8 for nomenclature) increases with the temperature by 0.01 Å (about 10σ), and the θ angle (figure 6) varies by 0.25 degree. The N...O distances which are involved in hydrogen bonds with adjacent PO_4 groups increase with temperature by 0.016, 0.019, 0.019 and 0.018 Å, for $x = 0.4$, 0.5, 0.8 and 0.9 respectively, when the temperature varies from 158 to 295 K. These variations are similar to those observed in pure ADP (0.020 Å) [18].

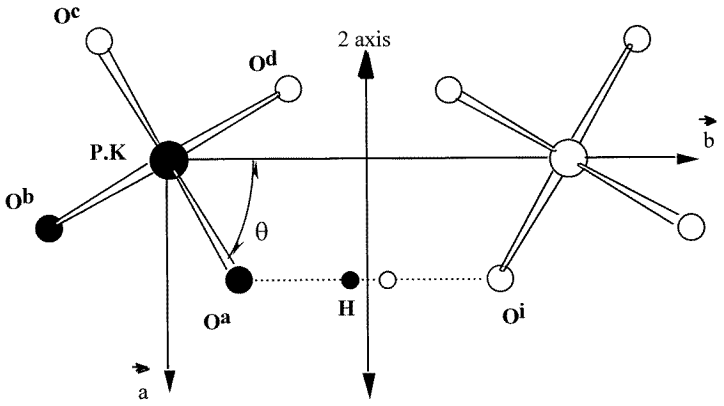

Figure 6. Projections of PO_4 group in (001) plane (see table 7 for nomenclature).

5.3. Variation of the stereochemical parameters with concentration

When x goes from 0 to 1, the main variations are the following: the O^a–P–O^b angle increases by 0.8° and O^a–P–O^c decreases by 0.4° ($\sigma = 0.02°$); the $N(K) \ldots O^{a,b,c,d}$ and $N(K) \ldots O^{e,f,g,h}$ (see tables 7 and 8) distances increase whatever the temperature; for example, at $T = 158$ K these distances are equal to 2.8424(5) and 2.9821(6) Å for $x = 0.4$ compared to 2.8896(2) and 3.1664(2) Å in ADP [18]. Then, $N \ldots O^{e,f,g,h}$ varies by more than 6%; the P–O...N(K) angle also increases from 98.70(1)° in KDP to 100.62(1)° for ADP (1.9%) while P...N(K)...O decreases by almost 8% (25.70° to 23.70(1)°).

Then, the increase of the c parameter with ammonium concentration results from the variation of the N–O interactions as well as from the variation of P–O...N(K) and P...N(K)...O angles. All these observations are in fact related to the bifurcated P–O...H–N hydrogen bonds which could play an important role in the mechanism of the phase transition [28].

Table 7. Bond distances (Å), angles (°) and standard deviations in $KADP_x$ ($x = 0.4$, 0.5, 0.8 and 0.9): (a) x, y, z; (b) $y, \bar{x}, \bar{z}$; (c) $\bar{x}, \bar{y}, z$; (d) $\bar{y}, x, 1-z$; (e) $1/2-x, y, 3/4-z$; (f) $\bar{y}, 1/2-x, 1/4+z$; (g) $-1/2+x, \bar{y}, 3/4-z$; (h) $y, -1/2+y, 1/4+z$; (i) $1/2-x, y, 3/4-z$.

	$KADP_{0.4}$			$KADP_{0.5}$			$KADP_{0.8}$			$KADP_{0.9}$			
	105 K	158 K	295 K	105 K	158 K	295 K	125 K	158 K	295 K	154 K	164 K	192 K	295 K
N–H(N)	0.94(1)	0.91(5)	1.03(3)	—	0.99(4)	—	1.01(1)	1.01(1)	0.97(1)	1.04(2)	1.02(2)	1.02(1)	1.03(2)
O–H(O)	1.04(3)	1.03(4)	1.05(3)	—	1.06(2)	—	1.06(2)	1.06(2)	1.06(1)	1.09(3)	1.10(3)	1.09(2)	1.08(3)
O–Oi	2.4784(5)	2.4794(7)	2.4881(10)	2.4771(6)	2.4785(7)	2.4847(13)	2.4745(6)	2.4757(6)	2.4837(5)	2.4750(8)	2.4761(8)	2.4753(8)	2.4820(11)
H(O)–H(O)	0.75(8)	0.70(9)	0.52(8)	—	0.39(5)	—	0.57(6)	0.54(5)	0.39(2)	0.35(5)	0.41(6)	0.40(4)	0.41(6)
P–Oa	1.5421(4)	1.5423(4)	1.5411(6)	1.5417(4)	1.5417(4)	1.5418(7)	1.5401(3)	1.5409(4)	1.5392(3)	1.5392(4)	1.5391(4)	1.5389(4)	1.5384(6)
N–O[e,f,g,h]	2.8424(5)	2.8481(5)	2.8648(6)	2.8569(5)	2.8569(5)	2.8756(7)	2.8744(4)	2.8791(3)	2.8985(3)	2.8831(5)	2.8839(5)	2.8868(5)	2.9012(6)
N–O[a,b,c,d]	2.9821(6)	2.9886(6)	3.0020(8)	3.0197(6)	3.0197(6)	3.0406(10)	3.1065(4)	3.1102(5)	3.1170(4)	3.1312(6)	3.1311(6)	3.1327(5)	3.1365(7)
H(N)–O[f]	1.94(5)	2.03(6)	1.88(3)	1.95(4)	1.95(4)	1.97(4)	1.99(2)	1.99(1)	2.06(1)	1.92(2)	1.96(3)	1.96(2)	1.99(3)
O–P–O[b]	108.76(2)	108.80(2)	108.82(3)	108.72(2)	108.72(2)	108.77(4)	108.59(2)	108.59(2)	108.68(1)	108.49(2)	108.50(2)	108.54(2)	108.55(3)
O–P–O[c]	110.91(3)	110.83(3)	110.79(4)	110.98(3)	110.98(3)	110.89(5)	111.24(2)	111.19(2)	111.07(2)	111.46(3)	111.43(3)	111.35(2)	111.33(3)
P–O–N	99.34(2)	99.45(2)	99.61(3)	99.57(2)	99.63(2)	99.87(3)	100.23(2)	100.25(1)	100.44(1)	100.31(2)	100.32(2)	100.39(2)	100.44(3)
P–N–O	25.21(1)	25.14(1)	24.99(1)	24.91(1)	24.88(1)	24.68(1)	24.15(1)	24.14(1)	24.03(1)	23.97(1)	23.96(1)	23.94(1)	23.89(1)
P–O–H(O)	108(2)	109(3)	112(2)	112(2)	112(2)	112(2)	106(2)	116(1)	110(1)	111(1)	114(1)	112(1)	112(2)
N–H(N)–O	153(3)	147(4)	158(4)	—	151(2)	—	145(1)	146(1)	144(1)	152(1)	150(1)	149(1)	147(2)
O–H(O)–O[i]	151(4)	154(5)	163(5)	—	172(3)	—	159(3)	161(2)	170(1)	164(2)	161(3)	161(1)	162(3)
H(N)–N–H(N)[b]	108(3)	114(5)	103(3)	—	111(3)	—	115(2)	114(1)	114(1)	112(1)	113(2)	113(1)	114(2)
H(N)–N–H(N)[c]	110(3)	100(4)	122(3)	—	106(2)	—	99(1)	102(1)	101(1)	105(1)	102(1)	102(1)	101(2)
θ	60.59(1)	60.52(1)	60.39(2)	—	60.43(1)	—	60.30(1)	60.25(1)	60.02(1)	60.23(2)	60.24(1)	60.17(2)	60.01(2)

Table 8. Bond distances, angles and standard deviations for ADP and KDP.

	ADP [18[b]] 158 K	ADP [29] 152 K	ADP [28] neutron 158 K	KDP [17] 127 K	KDP [17] 295 K
N–H(N)	0.99(1)	0.94(1)	1.002(5)		
O–H(O)	1.07(1)	1.13(2)	1.049(3)	1.0712(7)	1.0677(16)
O–O[i]	2.4776(4)	2.4858(9)	2.471(4)	2.4829(4)	2.4946(6)
H(O)–H(O)	0.33(3)	0.26(4)	0.377(5)	0.3428(12)	0.3647(28)
P–O[a]	1.5399(2)	1.5395(5)	1.538(2)	1.5429(3)	1.5403(4)
N–O[e,f,g,h]	2.8896(2)	2.9004(4)	2.889(3)		
N–O[a,b,c,d]	3.1664(3)	3.1298(6)	3.172(4)		
H(N)-O[f]	1.95(1)	2.01(2)	1.943(6)		
O–P–O[b]	108.52(1)	108.80(2)	108.57(4)	108.92(1)	108.95(1)
O–P–O[c]	111.39(1)	110.8(3)	111.29(7)	110.58(3)	110.52(3)
P–O–N(K)	100.62(1)		100.76(4)	98.57(1)	98.86(1)
P–N(K)–O	23.70(1)		23.60(4)	25.62(1)	25.88(1)
P–O–H(O)	115.6(6)	121(1)	116.3(2)	112.34(6)	112(1)
N–H(N)–O	157.7(6)		156.4(4)		
O–H(O)–O[i]	178(1)	169(2)	176.5(5)	178.22(16)	177.23(40)
H(N)–N–H(N)[b]	108(1)	107(1)	109.2(5)		
H(N)–N–H(N)[c]	112.3(6)	115(1)	109.6(2)		
θ	60.03(1)	60.04(1)	60.16	60.98(1)	60.89(1)

6. Mean square displacement parameters: analysis and discussion

The most important feature in these compounds is the variation of mean square displacement amplitudes with ammonium concentration: for all temperatures, the anisotropic thermal vibration along the $\boldsymbol{c}$ axis present a maximum for x close to 0.5.

6.1. Variation of U^{ii} with temperature

U^{11}, U^{22} and U^{33} for all P, O, N(K) atoms vary linearly with temperature (figure 7), showing quasiharmonic mean square displacements for all concentrations studied. For harmonic or nearly harmonic mean square displacements, each U parameter should be proportional to the temperature in the high-temperature limit [15]; then, one can write U as

$$U(T) = U_{stat} + U_{dyn}(T)$$

where U_{stat} is the extrapolation of the mean square displacement at $T = 0$ K: it represents the static disorder of the atom at $T = 0$ K. $U_{dyn}(T)$ is proportional to T, and can be related to the dynamical behaviour of the vibration that almost vanishes at $T = 0$ K. Then if, for example, an atom is moving along the $\boldsymbol{c}$ axis in a double-minimum potential well with minima Δ apart, we expect U_{stat} to be equal to $(\Delta/2)^2$. By inspection of U^{33}, Nelmes *et al* [15, 16] showed that for KDP, P and O atoms occupy two different sites along the $\boldsymbol{c}$ axis for which the largest distance is $\Delta = 0.1$ Å for the P atom. On the other hand, the extrapolation of U^{11} (U^{22}) at zero temperature was found very small, assigned to the zero-point vibration [15, 16].

Our results on mixed crystals agree quite well with those of Nelmes *et al* [15, 16]. For the P and O atoms, the extrapolations of U^{11} (U^{22}), at $T = 0$ K, are small and independent of concentration (table 9); along the $\boldsymbol{c}$ axis, the variation of U^{33} with concentration is surprisingly high: $\Delta(P)$ varies from 0.11 ($x = 1$) to 0.31 Å ($x = 0.5$) and Δ (O) goes

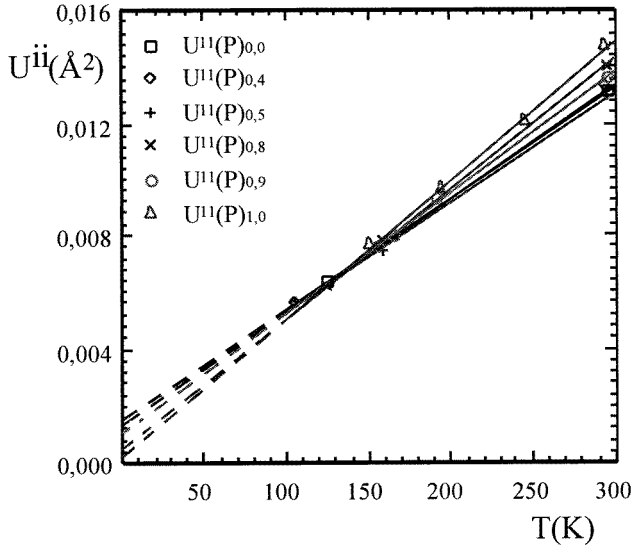

(a)

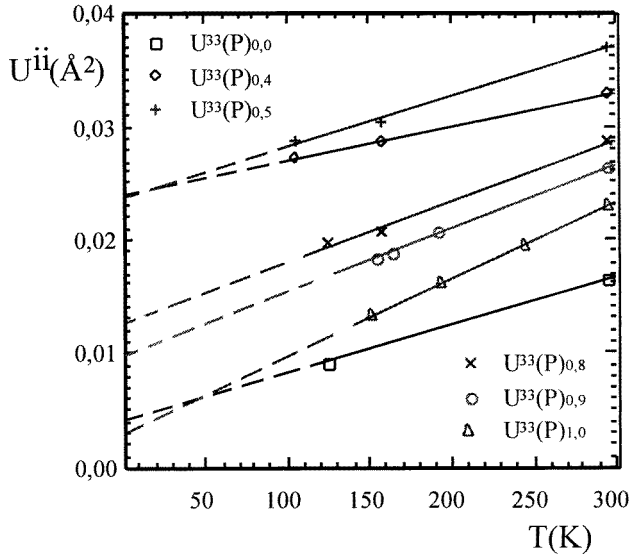

(b)

Figure 7. Variation of (a) U^{11}(P) and (b) U^{33} (P) with temperature ($x = 0, 0.4, 0.5, 0.8, 0.9, 1$).

from 0.09 to 0.28 Å. This extrapolation at $T = 0$ K, which leads to a large value of U^{33}, demonstrates that the static disorder of the PO_4 group increases with concentration. These results agree with those obtained from neutron inelastic scattering [30–32] which showed that the PO_4 tetrahedron has a large vibration along ***c***. This disorder does not show up clearly on the diffraction pattern; no satellite peaks and no significant diffuse scattering appear.

Table 9. Δ_{11} and Δ_{33} distances (Å) between the two atomic sites of P, O against x concentration along $\boldsymbol{a}$ and $\boldsymbol{c}$ directions.

	P		O	
x	Δ^{11}	Δ^{33}	Δ^{11}	Δ^{33}
0.0	0.08	0.13	0.08	0.09
0.4	0.07	0.31	0.09	0.28
0.5	0.08	0.31	0.10	0.28
0.8	0.05	0.22	0.08	0.21
0.9	0.07	0.20	0.09	0.17
1.0	0.03	0.11	0.02	0.09

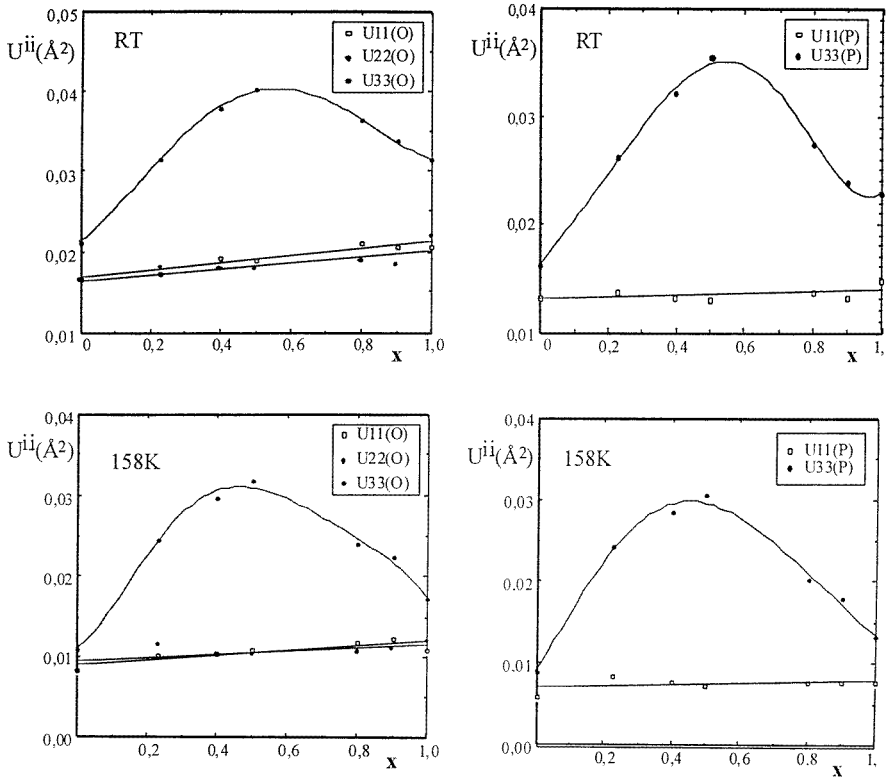

Figure 8. Variation of U^{ii}(O), U^{ii}(P) with concentration at room temperature and at $T = 158$ K.

6.2. Variation of U^{ii} with concentration

It is interesting to analyse mean square displacements against x at fixed temperature. Figure 8 gives the variation of U^{ii} for the P and O atoms at room temperature and at $T = 158$ K (the KDP values are extracted from the papers of Nelmes *et al* [15, 17]). The behaviour of U^{11}, U^{22} of P and O is almost linear with x whereas we observe a negative parabolic shape in the U^{33} case, with a maximum for $x = 0.5$. For K or N, U^{ii} parameters show the same feature with slightly less accuracy.

We can also write U^{33} as the sum of the static and dynamic components of the mean

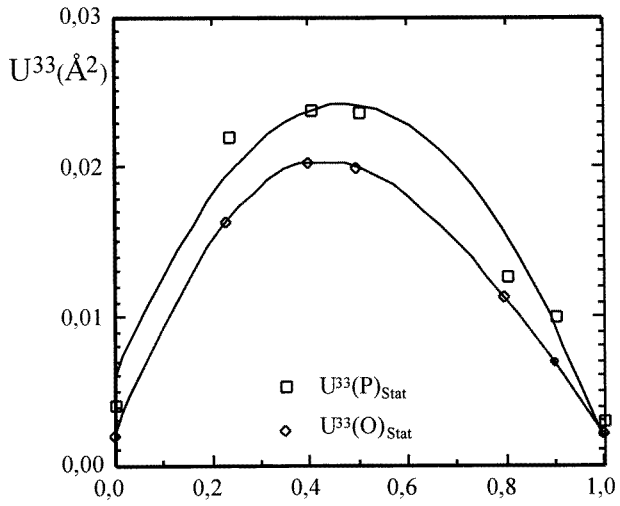

(a)

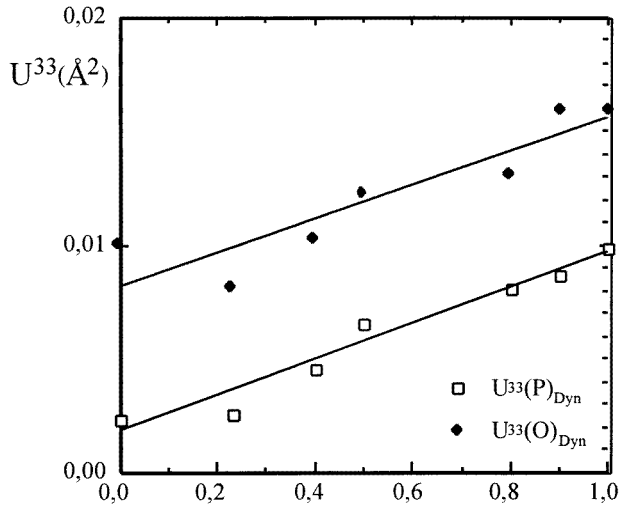

(b)

Figure 9. (a) Static and (b) dynamic parts of U^{33}(P) and U^{33}(O) against x at $T = 158$ K.

square anisotropic displacement parameters along $\boldsymbol{c}$:

$$U^{33} = U^{33}_{stat} + U^{33}_{dyn}.$$

The static U^{33}_{stat} and dynamic U^{33}_{dyn} components against concentration are shown in figure 9 ($T = 158$ K). The static one has a parabolic shape, while the dynamic is mostly linear as x goes from 0 to 1. Then, the non-linear behaviour is attributed to the static part only. Furthermore, when the ratio $U^{33}_{stat}/U^{33}_{dyn}$ for both O and P is close to two, the glassy phase appears. In conclusion, we have shown that, in the paraelectric phase of $K_{1-x}(NH_4)_xH_2PO_4$, the differences in bond lengths, intermolecular interactions and angles as a function of T or x are not contrasted enough within the phase diagram to understand

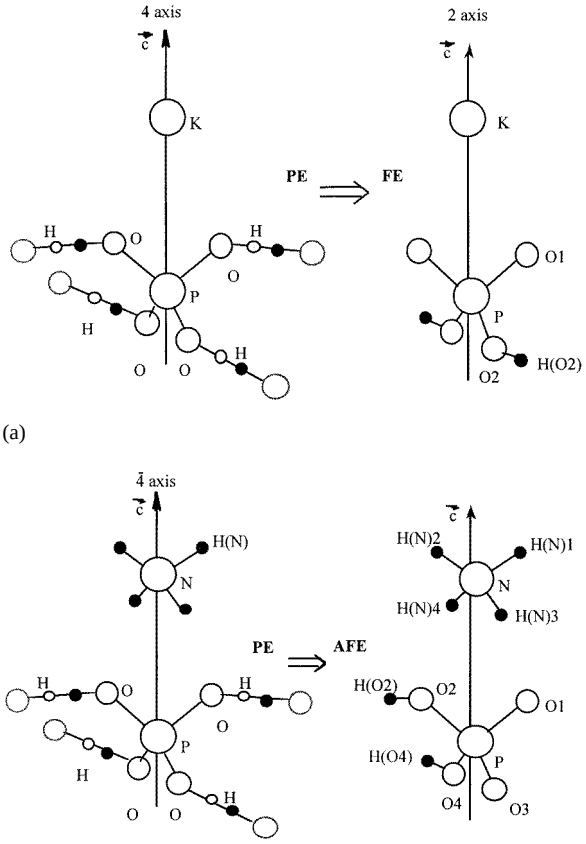

Figure 10. KH_2PO_4 and $(NH_4)H_2PO_4$ units: (a) paraelectric phases, (b) ferro- (antiferro-) electric phases.

the appearance of the glassy phase. Only a careful study of the thermal parameters allows some conclusions. When the static part of U^{33} of the atoms is predominant, the disorder to order transition cannot occur and a glassy phase appears. In that sense, U^{33} may be considered as the order parameter. Hydrogen bonds play an important role in the phase transition: figure 10 gives the structural arrangement of KDP and ADP in their paraelectric and ferro(antiferro)electric phases. In $KADP_x$ and for x greater than 0.8, the $(NH_4)^+$ ion imposes the H_2PO_4 configuration when the phase transition occurs (as in ADP): the four hydrogen bonds between the ammonium and the neighbouring PO_4 groups in the paraelectric phase (figures 4, bottom, and 11) are reduced to two after the transition imposing the $H_2PO_4^-$ configuration. In KDP and for solid solutions with $x < 0.23$ the K^+ interacts with $H_2PO_4^-$ by coulombic forces. When the transition occurs, in contrast to ADP, the K^+ ion (0, 0, 1/2) does not impose the configuration of the $H_2PO_4^-$ groups. The configuration adopted is the most stable one of the $H_2PO_4^-$ ion itself [33]. In the intermediate region of the phase diagram competition between the ferro- and antiferroelectric states occurs (i.e. between the two H_2PO_4 configurations); therefore, crystallographically, this frustration leads to the observed static disorder of the H_2PO_4 group which prevents the phase transition from occurring and which is revealed by the behaviour of U^{33}.

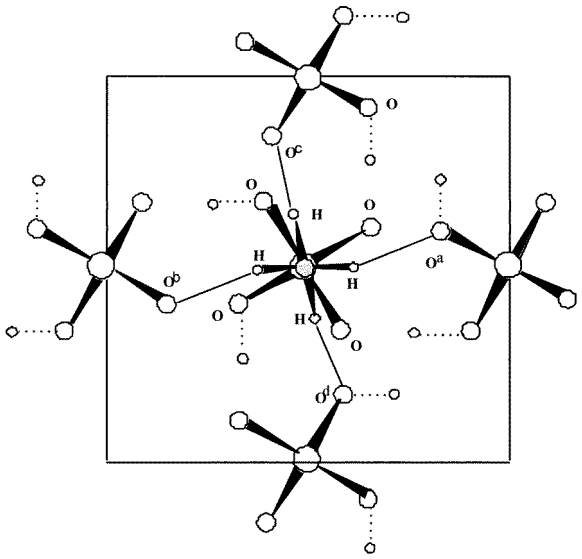

Figure 11. Projections of PO_4 and (NH_4) groups in the (001) plane. (a) $1/2 + x$, $\bar{y}$, $3/4 - z$; (b) $-1/2 + x$, $\bar{y}$, $3/4 - z$; (c) $\bar{x}$, $1/2 + y$, $1/4 - z$; (d) $\bar{x}$, $-1/2 + y$, $1/4 - z$.

Further work to explore the boundaries of the antiferro–glass and ferroelectric–glass regions by x-ray, neutron and IR techniques is under way.

Acknowledgments

We are grateful to CNRS and CNR for a joint cooperative grant (No 4552) between France and Morocco. A Boukhris is grateful to University Henri Poincaré for an invited Maître de Conférences position.

References

[1] Busch F and Scherver P 1935 *Naturewissenschaften* **23** 737
[2] Bacon G E and Pease R S 1953 *Proc. R. Soc.* A **220** 397
[3] Bacon G E and Pease R S 1955 *Proc. R. Soc.* A **230** 359
[4] Keeling R O and Pepinski R 1955 *Z. Kristallogr.* **106** 236
[5] Tenzer L, Frazer B C and Pepinsky R 1958 *Acta Crystallogr.* **11** 505
[6] Fukami T, Akahoshi S, Hukuda K and Yagi T 1987 *J. Phys. Soc. Japan* **56** 4388
[7] Fukami T, Akahoshi S, Hukuda K and Yagi T 1987 *J. Phys. Soc. Japan* **56** 2223
[8] Courtens E 1987 *Ferroelectrics* **72** 229
[9] Ono Y, Hikita T and Ikeda T 1987 *J. Phys. Soc. Japan* **56** 577
[10] Gridnev S A, Korotkov L N, Rogova S P, Shuvalov L A and Fedosjuk R M 1991 *Ferroelectrics* **13** 67
[11] Ono Y, Hikita T and Ikeda T 1988 *Ferroelectrics* **79** 327
[12] Ono Y and Yamada N 1991 *J. Phys. Soc. Japan* **60** 533
[13] Vaezzadeh B, Bréhat F and Wyncke B 1992 *J. Phys.: Condens. Matter* **4** 7401
[14] Boukhris A, Lecomte C, Wyncke B, Bréhat F and Thalal A 1994 *J. Phys.: Condens. Matter* **6** 2475
[15] Nelmes R J, Meyer G M and Tibballs J E 1982 *J. Phys. C: Solid State Phys.* **15** 59
[16] Nelmes R J 1987 *Ferroelectrics* **71** 87
[17] Nelmes R J, Tun Z and Kuhs W F 1987 *Ferroelectrics* **71** 125
[18] Boukhris A 1995 *Thèse de Doctorat d'Etat* University of Marrakech and University Henri Poincaré
[19] 1989 *Enraf Nonius User's Manual* (Delft)

[20] Blessing R H 1987 *Cryst. Rev.* **1** 3
[21] De Titta G 1985 *J. Appl. Crystallogr.* **18** 75
[22] McCandlish E, Stout G H and Andrews L S 1975 *Acta Crystallogr.* A **31** 245
[23] Sheldrick G M 1976 *SHELX 76, Program for Crystal Structure Determination* (Cambridge: University of Cambridge)
[24] Gabe E J, Lee F Li and Lepage Y *Crystallographic Computing 3* ed G M Sheldrick, C Krüger and R Goddard (Oxford: Clarendon) pp 164–74
[25] Hansen N K and Coppens P 1978 *Acta Crystlogr.* A **34** 909
Lecomte C 1991 *NATO-ASI B Physics* vol 250, ed G A Geffrey and J F Piniella (New York: Plenum) pp 121–53
[26] Clementi E and Raimondi D L 1963 *J. Chem. Phys.* **38** 2686
[27] Pérès N, Boukhris A, Souhassou M, Gavoille G and Lecomte C *Acta. Cryst.* B to be submitted
[28] Pérès N, Souhassou M, Gavoille G, Cousson A, Paulus W and Wyncke B 1997 *J. Phys.: Condens. Matter* **9** 6555
[29] Fukami T, Akahoshi S, Hukuda K and Yagi T 1987 *J. Phys. Soc. Japan* **56** 4388
[30] Belushkin A V, Tomkinson J, Shuvalov L A and Fedosyuk R M 1993 *J. Phys. Soc. Japan* **62** 403
[31] Belushkin A V, Tomkinson J, Shuvalov L A and Fedosyuk R M 1993 *Z. Phys.* B **90** 135
[32] Belushkin A V, Cadile J and Shuvalov L A 1993 *Europhys. Lett.* **22** 701
[33] Pauling L 1953 *J. Am. Chem. Soc.* **57** 2680
Fujii K 1994 *J. Phys. Soc. Japan* **63** 1572